

Time-Series JEPA for Predictive Remote Control under Capacity-Limited Networks

Abanoub M. Girgis, *Student Member, IEEE*, Alvaro Valcarce, *Senior Member, IEEE*, and Mehdi Bennis, *Fellow, IEEE*

Abstract—In remote control systems, transmitting large data volumes (e.g. video feeds) from wireless sensors to faraway controllers is challenging when the uplink channel capacity is limited (e.g. RedCap devices or massive wireless sensor networks). Furthermore, the controllers often only need the information-rich components of the original data. To address this, we propose a Time-Series Joint Embedding Predictive Architecture (TS-JEPA) and a semantic actor trained through self-supervised learning. This approach harnesses TS-JEPA’s semantic representation power and predictive capabilities by capturing spatio-temporal correlations in the source data. We leverage this to optimize uplink channel utilization, while the semantic actor calculates control commands directly from the encoded representations, rather than from the original data. We test our model through multiple parallel instances of the well-known inverted cart-pole scenario, where the approach is validated through the maximization of stability under constrained uplink channel capacity.

Index Terms—Joint-Embedding Predictive Architecture (JEPA), Time-series, predictive control, semantics.

I. INTRODUCTION

Semantic communication stands as a cornerstone in enabling 6G applications [1], ranging from autonomous vehicles [2] to smart cities [3] and augmented reality [4]. Its significance is underscored by its ability to facilitate intelligent and context-aware interactions among devices and systems. As 6G unfolds with its focus on ultra-reliable low-latency communication (URLLC) [5] and massive machine-type communication (mMTC) [6], semantic communication emerges as a vital for efficiency, reduced network congestion, and improved user experiences. By surpassing traditional data-centric paradigms, semantic communication extracts and leverages the intrinsic meaning embedded within transmitted data, enabling more intelligent interactions and decision-making processes.

Amidst the proliferation of interconnected devices in mMTC applications, efficient data processing and transmission are crucial. Semantic communication facilitates meaningful information exchange and motivates the development of intelligent edge computing frameworks. This localization mitigates latency and enhances real-time responsiveness, crucial for URLLC applications like autonomous vehicles. Moreover, semantic communication augments the capabilities of artificial intelligence (AI) and machine learning (ML) algorithms within

A. M. Girgis and M. Bennis are with the Centre for Wireless Communications, University of Oulu, Oulu 90014, Finland (e-mail: abanoub.pipaoy@oulu.fi; mehdi.bennis@oulu.fi).

A. Valcarce is with the Nokia Bell Labs, Massy, France (e-mail: alvaro.valcarce@nokia-bell-labs.com).

a communication network, leading to more accurate predictive analytics and proactive network management.

However, while traditional approaches to semantic communication primarily relied on generative models like auto-encoders, their tendency to reconstruct every detail of the transmitted signal poses challenges. In practical applications, downstream tasks often require only a subset of the information present in the original data. Consequently, reconstructing the entire dataset can introduce unnecessary computational overhead and increased latency, negating some of the benefits of semantic communication. Moreover, the computational complexity associated with training and deploying generative models presents scalability constraints, particularly for resource-constrained devices of many 6G applications.

To address these challenges, recent advancements in semantic communication have focused on enhancing communication efficiency and effectiveness in achieving task-specific goals. Unlike conventional supervised learning, self-supervised learning empowers models to learn meaningful representations directly from data without explicit supervision. Joint embedding approaches [7], [8], in particular, are designed to learn shared representations capturing both semantic features and underlying interrelationships across data. By jointly optimizing the encoding and decoding processes, these approaches effectively disentangle essential semantic information from raw data, while discarding redundant or irrelevant details. This not only enhances the efficiency and accuracy of semantic communication but also ensures seamless integration with critical downstream tasks.

Despite its promise, joint embedding-based semantic communication faces challenges regarding communication, control stability, and scalability. Semantic communication relies on joint embedding models to transmit encoded semantic representations across 6G devices. This can strain the control stability of numerous devices, especially under limited communication resources and adverse channel conditions. Incorporating the Joint-Embedding Predictive Architecture (JEPA), an extension of conventional joint embedding approaches tailored to predict one semantic representation from another, addresses these challenges. By infusing predictive components into the joint embedding framework, JEPA captures inherent relationships and dependencies within the data while predicting future semantic representations and transitions with the embedding space. This enables more accurate and dynamic semantic communication, laying a robust foundation for the intricate demands of 6G applications.

Motivated by this, this article presents a scheduling ap-

proach for multi-device control systems, integrating self-supervised learning [9]–[11] and split learning [12]. Our approach comprises two key components: (i) the *Time-Series Joint-Embedding Predictive Architecture (TS-JEPA)* model for extracting semantic representations and predicting missing ones, and (ii) the *semantic actor* for predicting control commands from semantic representations. The TS-JEPA architecture consists of both online and target networks, with the online networks comprising an encoder and predictor, and the target network featuring a momentum encoder with distinct weights. Unlike existing JEPA models [10], [13], TS-JEPA processes two augmented views over time and conditions the predictor on control commands. Training involves optimizing a loss function capturing similarities between augmented frames over time, with the model split between the sensor and controller ends. Pre-training TS-JEPA model precedes training the semantic actor. A channel-aware round-robin scheduler allocates radio resources to the devices based on channel conditions. This approach reduces communication costs and addresses scalability challenges in transmitting multi-device data under a capacity-limited network.

Simulation results on distinct inverted cart-pole systems demonstrate significant improvements with our proposed framework. It enhances average control and state predictions, achieving normalized errors of 0.52% and 2.9%, respectively at 20dB signal-to-noise ratio (SNR), (see Fig. 8-9 in Section V-A2). The framework also boosts scalability by 100% at 15dB SNR compared to the baselines. Moreover, leveraging predictive capabilities, it improves average control and state predictions, achieving normalized errors of 3.21% and 9.01%, respectively at five predictive time steps and 5dB SNR (see Fig. 10 in Section V-A3). Additionally, it demonstrates 103% scalability improvements at 5dB SNR relative to the baselines, showcasing robustness against decreasing SNR (Fig. 11 in Section V-A4).

A. Related Work

In modern 6G applications, optimizing communication resources for large-scale multi-device control systems is crucial. Various scheduling methods from static round-robin [14] to opportunistic [15] and control-aware scheduling [16], have been explored to enhance control performance under limited communication resources. However, while these approaches focus on resource utilization, there is a gap in addressing data transmission efficiency.

Recent advancements in AI and ML offer promising avenues for mitigating communication constraints in multi-device control systems. By leveraging the dynamics models of individual devices, these methods predict missing information from unscheduled devices, optimizing resource utilization. Time-series prediction models like long short-term memory (LSTM) [17] and gated recurrent unit (GRU) [18] show the potential to support more devices under limited bandwidth.

However, conventional methods suffer from communication and computational overheads, often requiring frequent model fine-tuning due to degraded prediction accuracy as a result of reconstructing raw data, intricate dynamics, and uncertainties

inherent in the systems. To address this, an integrated approach combines self-supervised learning [11] with predictive capabilities and split learning [12], reducing data volume transmission and improving scalability and efficiency.

B. Contributions and Organization

The major contributions of this article can be summarized as follows.

- We introduce a novel TS-JEPA framework for semantic control of multiple devices. It distills lower-dimensional semantic representations from sensory data and predicts missing representations at remote controllers, addressing the semantic control challenge.
- We propose that the semantic actor at the remote controller derives control commands based on the semantic representations provided by the TS-JEPA model.
- We introduce a semantic scheduler to iteratively select devices transmitting their semantic representations based on available wireless resources and channel states.
- We show through simulations on distinct inverted cart-pole systems that our proposed approach achieves comparable performance to baseline models with reduced communication and computation resources while maintaining control stability on multiple diverse devices.

The rest of this paper is organized as follows. In Section II, we describe the wireless multiple devices architecture and provide an overview of the JEPA in Section III. Section IV presents the proposed predictive remote control for multiple devices including the TS-JEPA model and semantic actor. In Section V, we numerically demonstrate the effectiveness and performance of the proposed approach for intelligent remote monitoring and controlling of multiple devices with application to inverted cart-pole systems. Finally, we conclude the work in Section VI.

II. SYSTEM MODEL

Consider controlling multiple distinct wireless dynamical systems comprising devices, sensors, and remote controllers as illustrated in Fig. 1. A device represents a combination of linear dynamic *process* being controlled and *actuator* applying control command on the process. The set size of devices is denoted by $|\mathcal{I}|$. Each device is associated with a *sensor* to sample the state of its process. The sampled states are transmitted to the remote controller, which has a high computational capability, to calculate the target control commands. The control commands are then sent to their associated actuators to drive the processes to their desired states.

The sensors deployed in this study generate high-traffic data volume due to their multi-dimensional characteristics, particularly in the case of pick-and-place devices within a smart factory. These devices could utilize advanced sensors and a vision system to enable self-perception capabilities. To achieve accurate state recognition, these devices rely on Ultra-HD high-frame-rate depth cameras, enabling detailed analysis of the device's joint positions and orientations. Control commands are then implemented based on the monitoring results, ensuring successful grasping, placement, and alignment of

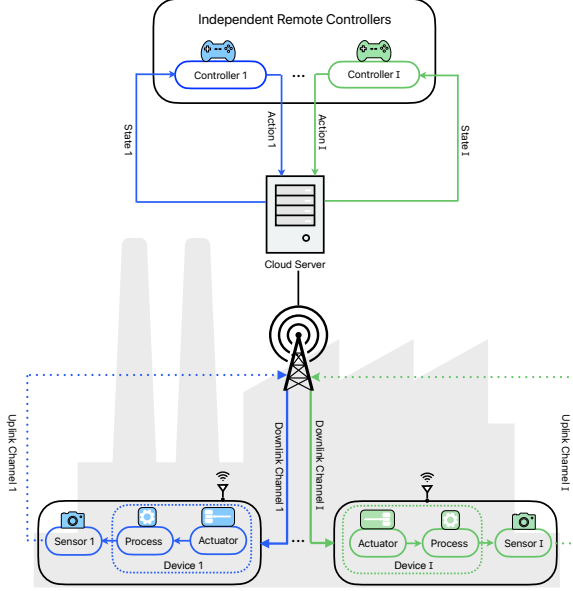


Fig. 1. A illustrative depiction of multiple different wireless devices operating under remote control of independent controllers in a smart factory.

objects, all without needing a physical presence on the factory floor thanks to wireless communications. Particularly, the sensor and device are co-located and share the same transceiver for wireless communication, while the remote controller is situated in a separate location, necessitating wireless uplink channels for communication with the sensors and controllers.

Transmitting high-dimensional system states from numerous sensors attached to diverse devices presents a challenge due to a limited-capacity network. To overcome this capacity limitation while retaining the input semantics, we leverage the *TS-JEPA*. The *TS-JEPA* differs from the source encoding methods by extracting low-dimensional *semantic* representations from sensor data, rather than just compressing it. This captures the essence of time-series sensory data, providing concise representations that address uplink capacity challenges. Beyond semantic representation extraction, the next representation predictor integrated within the *TS-JEPA* model endeavors to predict missing semantic representations at the controller side, attributable to constraints in capacity, errors in channels, bursts of interference, and unexpected shadows. This endeavor seeks to minimize the utilization of wireless communication resources. Furthermore, we introduce a *semantic actor* for predicting the control commands from the semantic representations within semantic space, which will be elaborated on in the next section. The scheduler iteratively allocates uplink wireless resources for multiple devices to transmit their semantic representations based on available wireless resources and channel conditions. Further details are described next to gain a more comprehensive understanding of the control and communication systems.

1) *Control System*: Consider a network of devices, each equipped with a sensor that samples the p -dimensional state at a fixed sampling rate τ_o . These state samples are then transmitted to the remote controller over wireless channels.

The sampled state of the device $i \in \mathcal{I}$ at time $t = k\tau_o$ is denoted by a vector as $\mathbf{x}_{i,k} \in \mathbb{R}^p$, for $k \geq 0$. Once the remote controller receives the state $\mathbf{x}_{i,k}$, it proceeds to calculate the optimal q -dimensional control command represented as a vector, denoted by $\mathbf{u}_{i,k} \in \mathbb{R}^q$. Subsequently, this calculated control command is transmitted to the associated actuator over an ideal channel. When the control command is applied on the device i , the evolution of its process's state can be mathematically represented as discrete linear time-invariant dynamics, given by [19]

$$\mathbf{x}_{i,k+1} = \mathbf{A}_i \mathbf{x}_{i,k} + \mathbf{B}_i \mathbf{u}_{i,k} + \mathbf{w}_{i,k}, \quad (1)$$

where $\mathbf{w}_{i,k} \in \mathbb{R}^p$ is a p -dimensional process noise vector of device i at time $t = k\tau_o$ whose entries are assumed to be independent and identically distributed (i.i.d.) Gaussian random variables with zero mean and variance N_s . The matrices $\mathbf{A}_i \in \mathbb{R}^{p \times p}$ and $\mathbf{B}_i \in \mathbb{R}^{p \times q}$ correspond to the linear time-invariant state transition and control matrices of device i , respectively. These matrices define the linearized dynamics of the process. We assume the state transition matrix \mathbf{A}_i is on its own unstable, i.e., it has at least one eigenvalue greater than unity. This is to say that, without a proper control command, the dynamics will drive the state $\mathbf{x}_{i,k} \rightarrow \infty$ as $k \rightarrow \infty$.

As illustrated in Fig. 1, the control loop of each system is closed through wireless channels. Hence, at each time $t = k\tau_o$, there are two distinct descriptions of process evolution in (1) depending on whether uplink transmission occurs or not. To capture this distinction, we introduce a binary variable $\beta_{i,k} \in \{0, 1\}$ to represent the event of a successful uplink transmission occurring for device i at time k . Then, the process evolution described in (1) can be presented as a switched linear evolution as

$$\mathbf{x}_{i,k+1} = \begin{cases} \mathbf{A}_i \mathbf{x}_{i,k} + \mathbf{B}_i \mathbf{u}_{i,k} + \mathbf{w}_{i,k}, & \beta_{i,k} = 1 \\ \mathbf{A}_i \mathbf{x}_{i,k} + \mathbf{B}_i \tilde{\mathbf{u}}_{i,k} + \mathbf{w}_{i,k}, & \beta_{i,k} = 0. \end{cases} \quad (2)$$

During the event of uplink transmission failure ($\beta_{i,k} = 0$), the actuator associated with device i at time k applies the predicted control command denoted as $\tilde{\mathbf{u}}_{i,k} \in \mathbb{R}^q$, which will be further detailed in Sec. IV. Conversely, during a successful uplink transmission ($\beta_{i,k} = 1$), the actuator applies the target control command calculated at the remote controller utilizing the linear quadratic regulator (LQR) approach [20], by solving the optimization problem formulated as

$$\mathbf{u}_{i,k}^* = \arg \min_{\mathbf{u}_{i,k}} \mathcal{J}(\mathbf{x}_k, \mathbf{u}_k) \quad (3)$$

subject to: (1),

$$\mathbf{u}_{min} \leq \mathbf{u}_{i,k} \leq \mathbf{u}_{max},$$

where $\mathcal{J}(\mathbf{x}_{i,k}, \mathbf{u}_{i,k}) = \frac{1}{2} \sum_{k=0}^{\infty} \mathbf{x}_{i,k}^T \mathbf{Q} \mathbf{x}_{i,k} + \mathbf{u}_{i,k}^T \mathbf{R} \mathbf{u}_{i,k}$ represents the quadratic cost function, \mathbf{Q} is a positive semi-definite weight matrix of the state deviation cost, and \mathbf{R} is a positive definite weight matrix of the control cost. Then, by solving problem (3) through dynamic programming [20], the optimal control command is expressed as

$$\mathbf{u}_{i,k} = \mathbf{K}_i (\mathbf{x}_{i,k} - \mathbf{x}_{i,d}), \quad (4)$$

where $\mathbf{K}_i \in \mathbb{R}^{q \times p}$ denotes the corresponding gain matrix, and $\mathbf{x}_{i,d} \in \mathbb{R}^p$ denotes the desired system state of device i .

Generally, applying the control command effectively closes the control loop, ensuring that the eigenvalues of the closed-loop dynamic matrix $\mathbf{A}_i^c := \mathbf{A}_i + \mathbf{B}_i \mathbf{K}_i$ are less than unity. On the other hand, when no uplink transmission occurs, the actuator applies the predicted control command utilizing the semantic actor to be detailed next. Moving forward, we will delve into the discussion of the wireless communication system, which plays a crucial role in determining the success of uplink transmission and ultimately closing the control loops.

2) *Wireless Communication System*: We consider a dense clutter and high base station Indoor Factory (InF-DH) scenario where different devices with irregular structures are randomly distributed within the coverage area of the base station. As depicted in Fig. 1, we assume the remote controllers to be located at a distant cloud server, while presuming the communication delay between these controllers and the base station to be negligible. Furthermore, the communication between the base station and devices is established through both control and data channels. Specifically, the data channels facilitate the exchange of data information, whereas the control channels are utilized to share state information, such as scheduling requests and grants. We adopt a discrete system model incorporating orthogonal frequency division multiple access (OFDMA) compatible with the 5G numerology with 15 KHz subcarrier spacing. The subcarriers are grouped into physical resource block (PRB), each consisting of 12 consecutive subcarriers over a transmission interval of 1ms. Such an architecture ensures a stringent latency bound of 1ms for the uplink of the system state to the remote controller. This latency constraint is indispensable for numerous industrial control systems, ensuring swift and responsive interactions critical for seamless operations [21]. At each time $t = k\tau_o$, the base station employs a radio resource scheduler to manage uplink channel access efficiently. Specifically, the base station grants channel access to individual devices by transmitting downlink control messages \mathcal{C}_i^d to each device. Hence, certain devices have the capability of transmitting their system states efficiently over the shared uplink channels, optimizing channel access utilization. It is assumed that the uplink and downlink control channels are error-free, free from contention or collision, and have a maximum capacity of C_{max} bits per second. This capacity enables the transmission of messages from a vocabulary set \mathcal{B} with a size of $2^{C_{max}}$.

The data channels are characterized by a standard path loss and a Rayleigh block fading model [22]. Specifically, the channel gains associated with different PRBs for a particular device remain constant throughout time τ_o but are i.i.d. across different times. Each device can be allocated any set of adjacent PRBs and the allocated PRBs for different devices are not overlapped. In the context of the InF-DH scenario, the line-of-sight (LoS) path loss between the i -th device and the associated remote controller is given as [23], [24]

$$PL_{dB}^{LoS} = 31.84 + 21.5 \log_{10} (D_i^{3D}) + 19 \log_{10} (f_c), \quad (5)$$

where D_i^{3D} is the 3-dimensional distance in meters between the i -th device and the associated remote controller, and f_c is the center frequency in GHz. Notably, a shadow fading standard deviation (std) value of 4.3 is considered in this model.

The LoS probability that determines whether the channel state is LoS or non-line-of-sight (NLoS) at a certain distance, is defined as

$$\mathbb{P}_{LoS} = \exp \left[- \frac{D_i^{2D}}{\frac{D_{clutter}}{\ln(1-\delta)}} \cdot \frac{h_{BS} - h_{i,R}}{h_c - h_{i,R}} \right] \quad (6)$$

where D_i^{2D} , $D_{clutter}$, δ , h_c , $h_{i,R}$, and h_{BS} are the 2-dimensional distance between i -th device and the remote controller, clutter size, clutter density, clutter height, antenna height of i -th device, and base station's antenna height. Additionally, the NLoS path loss between the i -th device and the remote controller is given as

$$PL_{dB}^{NLoS} = \max (PL_{dB}, PL_{dB}^{LoS}) \quad (7)$$

where the path loss PL_{dB} in (7) is given as [23], [24]

$$PL_{dB} = 33.63 + 21.9 \log_{10} (D_i^{3D}) + 20 \log_{10} (f_c), \quad (8)$$

with a shadow fading std value of 4.0. The NLoS path loss is vital in case of LoS conditions are obstructed or unavailable.

Considering data transmission from the i -th device to the remote controller at time $t = k\tau_o$, employing a fixed transmission power P_i , the received SNR from the i -th device over PRBs during time $t = k\tau_o$ can be denoted as

$$\gamma_{i,k} = 10^{-\frac{PL_{dB}^{NLoS}}{10}} \frac{P_i |H_{i,k}|^2}{N_c}, \quad (9)$$

where $H_{i,k}$ is the Rayleigh flat-fading channel gain between the device i and the remote controller over PRBs at time k and N_c is the additive white Gaussian noise (AWGN) power. Based on (9), the channel capacity of the uplink transmission of device i over PRBs during time k is expressed as

$$R_{i,k} = W_i \log_2 (1 + \gamma_{i,k}), \quad (10)$$

where W_i is the allocated bandwidth for transmission over a number of PRBs for device i . The outage of data transmission of device i during time k is an event where the uplink channel capacity drops below a predefined threshold, which is set to ensure the target transmission rate \bar{R} . Then, the outage probability is calculated as

$$\epsilon_{i,k} = \mathbb{P} [R_{i,k} < \bar{R}] = 1 - \exp \left[-10^{\frac{PL_{dB}^{NLoS}}{10}} \frac{N_c}{P_i} \left(2^{\frac{\bar{R}}{W_i}} - 1 \right) \right], \quad (11)$$

where (11) holds from the cumulative distribution function (CDF) of the exponential random variable. The outage probability is affected by the transmission power P_i , the allocated bandwidth W_i , and the distance from the device to the remote controller D_i^{2D} while the other communication parameters in (11) are given.

The proposed framework is intended to support massive networks, with a large number of devices. Contention-based channel access is not scalable for such scenarios, so our wireless network relies on a centrally controlled dynamic channel access mechanism. This mechanism operates as a centralized scheduler, determining which devices are granted access to each frequency resource. The scheduling decisions made by this mechanism are denoted by $\alpha_{i,j,k}$, where a value

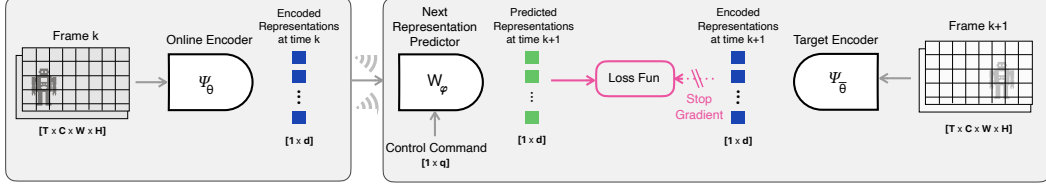


Fig. 2. Time-Series Joint-embedding predictive architecture (TS-JEPA) to extract semantic representations and predict missing semantic representations. Training operates on T consecutive frames with a spatial resolution $C \times W \times H$, encoded into a vector of size d .

of 1 indicates that device i is scheduled to transmit on PRB j at time k , while a value of 0 indicates otherwise. To precisely define these scheduling decisions, each device i has the flexibility to be allocated on a set of consecutive PRBs for transmission. To ensure collision-free transmissions, we enforce the constraint that at most one device transmits on each PRB j , expressed as $\sum_{i=1}^I \alpha_{ij,k} \leq 1$. Additionally, we allow each device to transmit on the J available PRBs, expressed as $\sum_{j=1}^J \alpha_{ij,k} \leq J$. Then, we formulate the transmission event $\beta_{i,k}$ of device i at time k , considering scheduling variables, transmission power, and channel states, as a Bernoulli random variable with a success probability characterized as

$$\mathbb{P}[\beta_{i,k} = 1 | H_{i,k}, \alpha_{i,k}] = 1 - \prod_{j=1}^J [(1 - \alpha_{ij,k}) + Q_{i,k}]. \quad (12)$$

where $Q_{i,k} = \alpha_{ij,k}(1 - \epsilon_{ij,k})$ represents the successful uplink transmission when the device i is scheduled at time k . The expression in (12) states that the probability of successfully receiving data from device i is commensurate with the probability of correctly receiving the transmitted data when the device i is designated to transmit on any of J available PRBs at time k . Note that we implicitly assume the absence of interference between transmissions on distinct PRBs.

III. JEPA-BASED SEMANTIC FRAME REPRESENTATION

This work leverages the JEPA to distill semantic representations from high-dimensional video frames, facilitating low-dimensional transmission [9], [10]. Additionally, the JEPA empowers predictive planning by extrapolating future representations through a comprehensive analysis of the optical flow within the semantic space. Incorporating self-supervised learning into the JEPA framework offers significant advantages. It allows the model to learn meaningful representations directly from data without explicit supervision, enhancing efficiency and reducing the need for labeled data. Leveraging inherent optical flow extracts rich semantic information and captures complex patterns. Moreover, self-supervised learning mitigates challenges related to data scarcity and annotation costs, particularly beneficial for large-scale video data tasks like semantic representation transmission.

1) *Joint Embedding Predictive Architecture*: Self-supervised learning epitomizes a method for representation learning, whereby a system endeavors to capture the intricate relationships embedded within its inputs. Conceptually, this endeavor aligns seamlessly with the framework of

energy-based models (EbMs), where the self-supervised objective entails assigning high energy to incompatible inputs and low energy to compatible ones. Existing non-generative approaches to self-supervised learning, such as Joint-Embedding Architecture (JEA) and JEPA, exemplify this pursuit. JEA strive to yield similar embeddings for compatible inputs and dissimilar embeddings for incompatible ones, typically leveraging randomly applied data augmentations on identical input images to construct compatible frame pairs in image-centric domains. However, a notable challenge with JEA lies in representation collapse, characterized by a flat energy landscape where the encoder yields a consistent output irrespective of input variation. To mitigate this collapse, several strategies have emerged, including contrastive losses that actively segregate embeddings of negative examples and non-contrastive losses aimed at minimizing redundancy across embeddings. Additionally, heuristic approaches exploit asymmetric architecture design to avoid collapse. In contrast, JEPA diverges from JEA by preventing the pursuit of representations invariant to a predefined set of data augmentations. Instead, JEPA endeavors to cultivate predictive representations conditioned on supplementary information. By learning to predict the embeddings of one signal from another compatible signal, JEPA employs a predictor network conditioned on additional information to facilitate prediction. Nonetheless, as with JEA, representation collapse remains a pertinent concern in JEPA, promoting adopting an asymmetric architecture design to prevent such issues, as elaborated further in subsequent paragraphs.

2) *Optical Flow Estimation*: The importance of optical flow estimation within the semantic space lies in its ability to provide insights into the spatial and temporal dynamics of objects in dynamic scenes, crucial for tasks like action recognition and object tracking. Integrating optical flow analysis enhances semantic representations, enabling more robust visual processing tasks. Indeed, motion is fundamental perception and facilitates various tasks such as robotics, navigation, and scene understanding. This section delves into the analysis of frame sequences depicting three-dimensional 3D scenes, where devices move while the camera remains stationary. Each point on the 3D surface follows a distinct 3D path within the camera-centric coordinate system, projecting onto the frame plane as a two-dimensional 2D path. These paths collectively form the 2D motion field, denoting the velocities of visible surface points. Optical flow estimation captures pixel-level motion across consecutive frames of a video sequence [25].

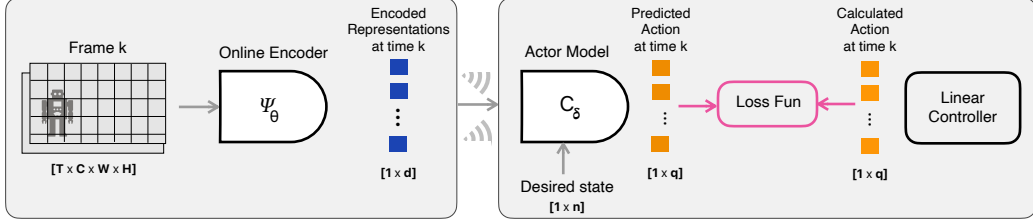


Fig. 3. Schematic representation of the semantic actor that calculates control commands based on semantic representations and desired state.

Given a pair of consecutive RGB frames as a function of spatial pixel space (x, y) and time k denoted as $\mathcal{I}_i(x, y, k)$ and $\mathcal{I}_i(x+v_1, y+v_2, k+1) \in \mathbb{R}^{3 \times W \times H}$, the corresponding optical flow $\mathcal{V} = (v_1, v_2) \in \mathbb{R}^{2 \times W \times H}$ estimates the apparent motion field of pixels from $\mathcal{I}_{i,k}$ to $\mathcal{I}_{i,k+1}$. Formally, optical flow can be expressed as the vector field $\mathcal{V} = (v_1(x, y), v_2(x, y))$, where x and y represent the spatial coordinates. The brightness constancy assumption governs optical flow, positing that pixel brightness remains constant between consecutive frames. This assumption leads to the optical flow constraint given as

$$\mathcal{I}_i^x v_1 + \mathcal{I}_i^y v_2 + \mathcal{I}_i^k = 0, \quad (13)$$

where \mathcal{I}_i^x and \mathcal{I}_i^y are the spatial derivatives of the image intensity with respect to x and y , and \mathcal{I}_i^k represents the temporal derivatives. Moreover, it assumes small movements between consecutive frames, approximated through a Taylor series, and spatial coherence, where points move similarly to their neighbors. Solving the constraint in (13) yields the approximated optical flow field. Various approaches have been proposed to estimate optical flow, each with its advantages and limitations. Classical methods like the Lucas-Kanada method rely on local brightness constancy and spatial gradients for optical flow computation [26]. Although computationally efficient, they may struggle with significant displacements or occlusions. In contrast, modern deep learning-based approaches leverage convolution neural networks (CNNs) to learn hierarchical representations directly from the raw frames [27]–[29]. However, these methods focus on pixel space optical flow estimation based on auto-encoder architectures.

IV. UNIFIED PREDICTIVE REMOTE CONTROL ACROSS MULTI-DEVICES

This section introduces a pioneering predictive remote control framework featuring two key models: TS-JEPA and *semantic actor* models. The TS-JEPA extracts the semantic representations from the high-dimensional frame at the sensor side and predicts missing semantic representation at the controller side. Then, the semantic actor computes control commands based on the semantic representations. This innovative approach enhances scalability across multi-device by reasoning and planning within the lower-dimension semantic space, a concept elaborated in detail next.

A. Time-Series Joint Embedding Predictive Architecture

The real-time remote monitoring procedure employing the proposed TS-JEPA model unfolds in two distinct phases.

During the first phase, devices transmit frames to remote controllers, deducing target control commands based on the received frames. These control commands subsequently drive the device's actuator toward the desired state. Concurrently, the proposed TS-JEPA model, depicted in Fig 2, undergoes training using the collected frames and their corresponding control commands. This first phase persists until the TS-JEPA model attains sufficient training. In the second phase, remote monitoring is performed based on semantic representations using the trained TS-JEPA model. By harnessing the trained TS-JEPA, the remote monitoring system achieves effective control across multiple devices without continuous frame transmission, making it suitable for remote control applications under a limited-capacity network.

Inspired by the JEPA [9] and diverging from the image-based JEPA [10], the proposed TS-JEPA aims to predict the next semantic representation of the next frame given the current frame. As illustrated in Fig. 2, the overall structure of the proposed TS-JEPA model is a tripartite model composed of an *online encoder* $\Psi_\theta(\cdot)$, *target encoder* $\Psi_{\bar{\theta}}(\cdot)$, and *next representations predictor* $W_\varphi(\cdot, \mathbf{u}_{i,k})$ conditioned on the control command $\mathbf{u}_{i,k}$. The online encoder, situated at the device, is characterized by a weight set θ , while the predictor, located at the remote controllers, is defined by a weight set φ . Moreover, the target encoder, also situated at the remote controllers, adopts a structure akin to the Bootstrap Your Own Latent (BYOL) approach [11], mirroring the architecture of the online encoder while employing different weights denoted by $\bar{\theta}$, signifying an exponential moving average (EMA) of the online parameter. Specifically, given a target decay rate $\eta \in [0, 1]$, after each training step the weights are updated as [11],

$$\bar{\theta} \leftarrow \eta\theta + (1 - \eta)\bar{\theta}. \quad (14)$$

The online encoder functions to embed the high-dimensional frame into a lower-dimensional semantic representation, while the target encoder provides regression targets to facilitate training of both the online encoder and predictor. Meanwhile, the next representation predictor facilitates planning by predicting future representations based on the current representation, conditioned on the control command.

To unravel the operational dynamics of the proposed TS-JEPA model, we initially delve into the second phase of remote monitoring, assuming the TS-JEPA is well-trained. Without loss of generality, we suppose that the second phase starts at

time $t = k\tau_0$. The TS-JEPA model's training procedures will be detailed subsequently. At the beginning of the second phase, the device's attached camera captures a frame depicting the device's state $\mathbf{x}_{i,k}$, whereby the online encoder derives semantic representations $\Psi(\mathbf{x}_{i,k})$ and transmits them wirelessly to the remote controllers. Subsequently, the semantic actor located at the remote controller predicts the control command $\tilde{\mathbf{u}}_{i,k}$ grounded on the received semantic representation, as explained in Section IV-B. The non-linear evolution of the semantic representations at the remote controllers given in (15) revealing the inherent within semantic space is obtained by conveying $\Psi(\mathbf{x}_{i,k})$ through the next representation predictor as

$$\tilde{\Psi}_\theta(\mathbf{x}_{i,k+1}) = W_\varphi(\Psi(\mathbf{x}_{i,k}), \mathbf{u}_{i,k}). \quad (15)$$

In broader context, predicting future semantic representations at time $t = (k+l)\tau_0$ is achieved by auto-regressively applying the next representation predictor l times as

$$\tilde{\Psi}_\theta(\mathbf{x}_{i,k+l}) = W_\varphi \circ W_\varphi(\Psi(\mathbf{x}_{i,k}), \mathbf{u}_{i,k}) \circ \cdots \circ W_\varphi, \quad (16)$$

for $l \in \mathbb{Z}_+$. Nonetheless, due to potential errors stemming from imperfect model training and other system noise, the prediction accuracy decreases with increasing prediction depth l . Consequently, rather than persisting with the same model after the first phase, it becomes imperative to revert to the first phase after a certain period to fine-tune the model for accurate representation prediction. Herein, the proposed TS-JEPA model serves a dual role: (i) extracting lower-dimensional semantic representations from high-dimensional data and (ii) predicting future semantic representations from the last received representations.

In the remote monitoring scenario, where the online encoder, target encoder, and predictor are spatially separated, their training for a number of epochs initially involves split learning. The first two frames at time k are fed into the online encoder, yielding its semantic representations $\Psi(\mathbf{x}_{i,k})$. Subsequently, the device transmits a tuple comprising the second pair of frames at time $k+1$ and the semantic representation at time k to the remote controllers over wireless channels. Here, the remote controllers utilize the received semantic representation at time k with the next representation predictor to derive the predicted next semantic representation $\tilde{\Psi}(\mathbf{x}_{i,k+1})$. Meanwhile, they apply the second pair of frames received at time $k+1$ to the target encoder, generating the target next semantic representation $\Psi(\mathbf{x}_{i,k+1})$. Notably, the online encoder exclusively employs the next representation predictor, enhancing asymmetric architecture between the online and target branches to prevent representation collapse. Concurrently, the remote controller transmits error feedback regarding the predicted representations over wireless channels. The device keeps transmitting the subsequent frames along with the current representations until the online encoder and next representation predictor are trained by minimizing the *cosine similarity* between the normalized predicted and target semantic representations given as

$$\mathcal{L}_{sim} = \frac{1}{K_s} \sum_{k=1}^{K_s} \frac{\langle \tilde{\Psi}(\mathbf{x}_{i,k+1}), \Psi(\mathbf{x}_{i,k+1}) \rangle}{\|\tilde{\Psi}(\mathbf{x}_{i,k+1})\|_2 \cdot \|\Psi(\mathbf{x}_{i,k+1})\|_2}, \quad (17)$$

where K_s denotes the number of samples observed in the first phase of remote monitoring. Note that the cosine similarity loss function employed in the TS-JEPA model, is non-contrastive, deviating from the loss function of the JEPA model, which typically utilizes energy minimization functions like mean squared error (MSE). The proposed TS-JEPA model is trained by minimizing the similarity loss function in (17) augmented with an l_2 regularization term on the model weights to avoid overfitting. Therefore, the minimization problem of the total loss function is addressed as

$$\arg \min_{\theta, \varphi} \mathcal{L}_{sim} + \|\mathbf{W}_j\|_2, \quad (18)$$

where \mathbf{W}_j represents the TS-JEPA model weights. The TS-JEPA model weights are trained using stochastic gradient descent (SGD) and backpropagation, with feedback transmitted from the remote controller to the device. Moreover, for seamless deployment of the TS-JEPA components across multiple devices, we employ a centralized training approach coupled with decentralized execution. This strategy entails centralized training of the TS-JEPA model, followed by a distribution to the other devices. However, training individual encoders for each device will be considered as future work.

B. Actor-Based Control Command Computation

In this section, we introduce a *semantic actor* situated at remote controllers, designed to predict control commands from semantic representations. The real-time remote control method employs this semantic actor shown in Fig. 3, consisting of two primary phases. During the initial phase, the device wirelessly transmits a tuple of frames alongside their semantic representations to the remote controller. Here, the controllers calculate target control commands based on the received frames, which are subsequently relayed back to the device's actuator, guiding it toward the desired state. Concurrently, the proposed semantic actor undergoes training using the collected semantic representations and corresponding control commands. The training phase continues until the semantic actor achieves sufficient efficiency. In the second phase, remote control operations rely on control prediction facilitated by the trained semantic actor, leveraging semantic representation. Here, the frame transmission from devices to remote controllers is unnecessary. Instead, in the remote control mode shown in Fig. 4(b), the semantic actor depends on received semantic representations, utilizing the encoding capabilities of the trained TS-JEPA model. Conversely, in the autonomous control model shown in Fig. 4(a), the semantic actor employs predicted semantic representations from the trained TS-JEPA model's next representations predictor. Through the synergy of the trained semantic actor and the TS-JEPA model, remote control systems achieve efficient control without the need for transmitting high-dimensional data.

The proposed semantic actor adopts Multi-layer Perceptron (MLP) structure denoted as \mathbf{C}_δ , conditioned on the desired state, illustrated in Fig. 3. Situated at the remote controllers, the semantic actor is characterized by a weight set δ . To first understand the operational structure of the proposed semantic actor, particularly in the second phase of remote control when

assuming its proficiency, we delve into its functionality. At the beginning of the second phase and the remote control mode, the trained online encoder at the device side transmits the semantic representation $\Psi_\theta(\mathbf{x}_{i,k})$ to the remote controllers over wireless channels. Then, the semantic actor predicts the control command $\tilde{\mathbf{u}}$ based on the received semantic representations, represented as $\tilde{\mathbf{u}}_{i,k} = \mathbf{C}_\delta(\Psi_\theta(\mathbf{x}_{i,k}))$. In the autonomous control mode, the semantic actor predicts the control command from the predicted semantic representations using the predicted next semantic representations, expressed as $\tilde{\mathbf{u}}_{i,k} = \mathbf{C}_\delta(\tilde{\Psi}_\theta(\mathbf{x}_{i,k}))$. However, owing to potential errors arising from imperfect model training, including both the TS-JEPA and semantic actor models, alongside other system noise such as random disturbances or uncertainties, prediction accuracy tends to decline with increasing prediction depth. Therefore, rather than persisting with the same models beyond the initial phase, it becomes imperative to return to the first phase. This allows for refining either the TS-JEPA or semantic actor model to attain a predefined level of accuracy in control command prediction.

In the remote control scenario, after training TS-JEPA model, the semantic actor at the remote controller receives a tuple consisting of frames and their corresponding semantic representations transmitted from the device. Concurrently, the remote controller sends back error feedback pertaining to the predicted control commands. The devices continue transmitting frames alongside semantic representations until the semantic actor is trained, aiming to minimize the mean absolute error (MAE) between the predicted control command $\tilde{\mathbf{u}}_{i,k}$ and target control command $\mathbf{u}_{i,k}$, defined as

$$\mathcal{L}_{act} = \frac{1}{K_c} \sum_{k=1}^{K_c} |\mathbf{u}_{i,k} - \tilde{\mathbf{u}}_{i,k}|, \quad (19)$$

where K_c represents the number of samples observed in the first phase of remote controlling. The proposed semantic actor is trained by minimizing the actor loss function in (19) augmented with an l_2 regularization term on the network weight to avoid overfitting. Hence, the minimization problem of the overall loss function is given as

$$\arg \min_{\delta} \mathcal{L}_{act} + \|\mathbf{W}_a\|_2, \quad (20)$$

where \mathbf{W}_a represents the semantic actor weights. The semantic actor weights are trained using Adam optimizer and back-propagation. Moreover, an early stopping strategy is exploited to avoid overfitting, enhancing prediction accuracy. Note that the device must regularly transmit the frames along with their corresponding semantic representations to the remote controllers over wireless channels in the first phase of remote controlling until the semantic actor is trained.

V. SIMULATION RESULTS

In this section, we evaluate the scalability and generality of the proposed predictive remote control approach across multiple inverted cart-pole systems controlled at a distance over a shared wireless channel. The choice of the inverted cart-pole system is deliberate, considering its simplicity, well-established status as a fundamental problem in control theory,

and its representation as a baseline use case. It is also a prime example of a robotic system amenable to remote control applications. Each system at a given time step is defined by an internal system state representing the horizontal cart's position and velocity and the pendulum's vertical angle and angular velocity. The control command is characterized by applying a horizontal force on the cart [30]. Utilizing a zeroth-order hold with a state sampling rate of 1 Hz on the continuous nonlinear dynamics, and linearizing it around the pendulum up position, with a pendulum angle ranges from $-\pi$ to π , yields the following discrete linear time-invariant dynamics matrices as

$$\mathbf{A}_i = \begin{bmatrix} 1 & 0.204 & -0.041 & -0.002 \\ 0 & 1.040 & -0.424 & -0.041 \\ 0 & 0.002 & 1.122 & 0.208 \\ 0 & 0.021 & 1.244 & 1.122 \end{bmatrix}, \mathbf{B}_i = \begin{bmatrix} 0.004 \\ 0.040 \\ 0.002 \\ 0.021 \end{bmatrix}. \quad (21)$$

Given the largest eigenvalues of \mathbf{A}_i , denoted as $\{1.00, 1.04, 1.62, 0.61\}$, exceed unity, it indicates the inherent instability in the inverted cart-pole system in the absence of suitable control commands. To rectify this, the feedback gain matrix \mathbf{K}_i is computed at the remote controller using the LQR approach in (4) with a state deviation cost of $\mathbf{Q} = \text{diag}\{1, 1, 1, 1\}$ and a control cost of $\mathbf{R} = 1$, aimed at stabilizing the inverted cart-pole system.

We examine **ten inverted cart-pole systems** featuring distinct target cart positions spanning the range $[-2.5, 2.0]$ and restricted to integer values, across a trajectory length of 100 time steps. Capturing internal system states poses a challenge, often demanding an array of sensors to ensure robust sensing and efficient data processing at the remote controller. This complexity arises from the requirement of precise and synchronized measurements of multiple variables simultaneously. Furthermore, the inherent uncertainties in sensor measurements present significant hurdles for estimation algorithms tasked with effectively determining the system's state. To streamline this process, we opt for a vision system with cameras to capture the cart-pole system state at each time step through RGB colour images with a resolution of 600×1200 pixels. The cameras, operate at a frame rate perfectly synchronized with the sampling rate, set at 1 frames per second (fps). For the wireless uplink from the sensor to the remote controller, we evaluate the performance of the proposed and baseline approaches based on various SNR values, specifically $\gamma_{i,k} \in \{5, 10, 15, 20\}$ dB. Additional parameters are detailed in Table I.

1) *Data Generation and Training:* The proposed TS-JEPA dataset is generated at the remote controllers, drawing upon calculated control commands and received depth frames from the distant cameras attached to the inverted cart-pole systems. These frames are captured at a frame rate of 1 fps over a trajectory length of 100 s. The system's initial conditions are randomly initialized from uniform distributions: $[-4.8, 4.8]$ for the cart position and $[-0.5, 0.5]$ for the other system state. For each initial condition, depth frames are collected based on (1) using the discrete linear time-invariant dynamics in (21). At the same time, control commands are computed via the

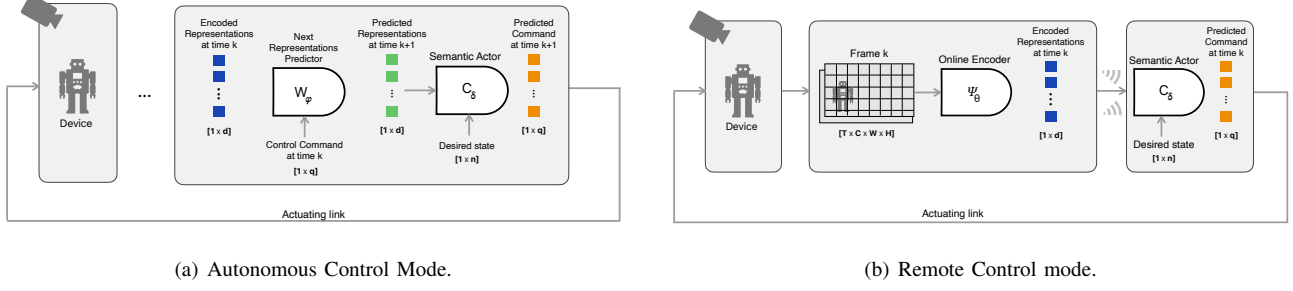


Fig. 4. Schematic representation of the different control modes based on either encoding or predicting capabilities.

optimal LQR controller detailed in (4), with $u_{max} = 25$ and $u_{min} = -25$.

To improve the generalization ability of learned semantic representations and prevent representational collapse, we introduce various input image augmentations as described next. These include color jittering, color dropping, Gaussian blurring, normalization, and resizing [8]. In color jittering, we introduce a random offset of 0.05 for brightness, 0.1 for contrast, 0.1 for saturation, and 0.05 for hue, applied uniformly to all pixels within the image. The sequence of these adjustments is randomly chosen for each patch. For color dropping, a probability of 0.05 of converting the image to grayscale, where the RGB pixel intensity is converted to its luma component. In Gaussian blurring, a square Gaussian kernel of size 5×5 is applied to resizing 128×128 frames, with a standard deviation uniformly sampled from the range $[0.1, 0.2]$. Finally, we normalize the color channels by subtracting the mean color values of $[0.485, 0.456, 0.406]$ and dividing them by the standard deviation of $[0.229, 0.224, 0.225]$. Since the object (i.e. the cart and pole) in our images move slowly, an excessively large frame rate may lead to consecutive image repetitions. Such a high frame rate is burdensome to the semantic encoder and poses overfitting risks to slowly changing states. To avoid this pitfall, we select the frame rate that yields a median mean absolute percentage error (MAPE) between consecutive frames above 1%. This way, we strike a balance between capturing sufficient temporal information and avoiding unnecessary computational costs. The MAPE between two consecutive frames in a dataset comprising K_f frames is defined as

$$MAPE = \frac{1}{K_f} \sum_{k=1}^{K_f} \left| \frac{\mathcal{I}_{i,k+1} - \mathcal{I}_{i,k}}{\mathcal{I}_{i,k}} \right| \times 100\%. \quad (22)$$

After applying image augmentations, the MAPE between frames is even larger, thus guaranteeing enough variance in the input images for training. This is illustrated in Fig. 5.

During testing, we exclusively utilize resizing and normalization as image augmentations. Since the control commands are input features to the next representation predictor, we apply z-score normalization for training stability reasons as follows:

$$\mathbf{u}_{i,k}^N = \frac{\mathbf{u}_{i,k} - \mu_u}{\sigma_u}, \quad (23)$$

where $\mathbf{u}_{i,k}^N$ signifies the normalized control command, while μ_u represents the mean of the control commands in the training

dataset, and σ_u represents the standard deviation of the control commands in the training dataset. Fig. 6(a) illustrates the training, validation, and test control commands, ranging from -25 to 25 , exhibit identical Gaussian distributions, each with a probability distribution function (PDF) of 0.3 centered around a zero mean. In contrast, Fig. 6(b) depicts normalized training, validation, and test control commands, confined within -10 to 10 , sharing similar Gaussian distributions across training, validation, and test datasets, each with a PDF of 0.85 around zero mean. This normalization practice ensures the stability of training the TS-JEPA model.

The proposed semantic actor dataset is constructed at the remote controller, incorporating calculated control commands, desired system states, and semantic representations of depth frame. These representations originate from the online encoder at the device during scheduled transmission or are predicted by the next representation predictor located at the remote controller. We perform training, validation, and testing using 200, 40, and 25 trajectories, each spanning a length of 100s at a frame rate of 1fps. Hence, the total number of samples comprising pairs of depth frames and associated control commands amount to 20000, 4000, and 2500 for training, validation, and testing, respectively, resulting in a training/validation/test split of 76/15/9. It is worth noting that trajectories are shuffled before training the TS-JEPA, however, samples within trajectories remain unshuffled during training to preserve potential temporal correlation between consecutive frames, ensuring the model learns temporal patterns based on the dataset order.

The encoder architecture in TS-JEPA model, consists of an initial 7×7 convolutional layer with 6 channels followed by 2×2 max pooling layer. The encoder comprises four residual blocks, each containing two 3×3 convolutional layers with increasing numbers of filters (64, 128, 256, 512) and shortcut connections that bypass one or more layers to mitigate the vanishing gradient problem. Batch normalization and rectifier linear unit (ReLU) activation functions are applied after each convolutional layer, and zero-padding is used to maintain feature map dimensions. The encoder architecture concludes with a global average pooling layer and MLP with an output layer of dimension 256 [11]. The predictor architecture in the TS-JEPA model is a MLP with a hidden layer of dimension 512 followed by a ReLU activation function and an output layer of dimension 256. The TS-JEPA model's weights and biases are trained to minimize the loss function in (17), utilizing the

TABLE I
SYSTEM PARAMETERS

Parameters	Symbol	Values
Hall Size		$300 \times 150 \text{ m}^2$
Room Height		6 m
BS Height	h_{BS}	10.0 m
Device Height	$h_{i,R}$	1.5 m
Carrier frequency	f_c	3.75 GHz
Total Bandwidth		20 MHz
Clutter height	h_c	3m
Clutter size	D_{clutter}	2.0 m
Clutter density	δ	60%
2D distance	D_i^{2D}	50 m
Noise power	N_c	-95 dB

TABLE II
TS-JEPA HYPER-PARAMETERS

Hyperparameters	Values
Learning rate (LR)	2×10^{-1}
Batch size	256
Epoch number	150
Optimizer	SGD
Weight decay	0.004
LR decay	Linear
LR decay factor	0.9
LR decay step size	10 epochs

TS-JEPA hyperparameters in Table. II.

The semantic actor is structured as a MLP, with an input layer that concatenates semantic representations and desired state, a hidden layer of dimension 1024, and an output layer of dimension 1, corresponding to the control command. All layers, excluding the output, employ a ReLu activation function. The semantic actor's weights and biases are optimized by minimizing the loss function in (19), leveraging the hyperparameters specified in Table III.

2) *Baseline Models*: : The performance of the proposed predictive remote control approach in Section. IV is compared to two baselines. In **Baseline 1 (Static round-robin scheduling w/o TS-JEPA)**, the sensors attached to devices regularly transmit high-dimensional data (i.e. images) to remote controllers in a predefined order, irrespective of prevailing channel conditions. The controller employs the most recent outdated state received when a device is unscheduled or experiences unfavorable channel conditions. Otherwise, it applies the control command based on the latest received state. In **Baseline 2 (Channel-aware round-robin scheduling w/o TS-JEPA)** the sensors regularly transmit high-dimensional data to remote controllers, considering current channel conditions fluctuating over time and influenced by environmental changes and nearby object movements. Channel-aware scheduling adjusts uplink transmission priorities based on channel conditions to optimize system performance. In unfavorable conditions, the controller utilizes the most recent outdated state, Otherwise relying on

TABLE III
SEMANTIC ACTOR HYPER-PARAMETERS

Hyperparameters	Values
Learning rate	6×10^{-3}
Batch size	200
Epoch number	300
Optimizer	Adam
Dropout	0.2

the latest state received.

3) *Evaluation Metrics*: : The performance evaluation of the proposed predictive remote control approach involves two aspects: assessing the encoded semantic representations of the TS-JEPA model through t-Distributed Stochastic Neighbor Embedding (t-SNE) and evaluating the semantic actor using the normalized mean absolute error (NMAE) of its predictions. The t-SNE serves to simplify the complexity of high-dimensional data while preserving most of its essential features, enabling a deeper understanding of the encoded semantic representations. By persevering the local structure of the high-dimensional representations, where similar representations in the original space remain close to each other in the reduced dimensionality, t-SNE provides valuable insights into the intrinsic structure of the representations. Meanwhile, the semantic actor's performance is measured by computing the NMAE between the predicted and actual control commands, quantifying the discrepancy in control predictions over multiple time steps, given as

$$\mathcal{N}_{i,K_p}^u = \frac{\frac{1}{K_p} \sum_{k=K_s+1}^{K_s+K_p} |\tilde{u}_{i,k} - u_{i,k}|}{|\max(u) - \min(u)|}, \quad (24)$$

where \mathcal{N}_{i,K_p}^u refers to the NMAE of the device i at time k for K_p control prediction time steps during testing. The denominator of (24) signifies the absolute difference between the maximum and minimum control commands in the training dataset. Moreover, to evaluate the effectiveness of the predicted control command upon their application to the device, we utilize the normalized root mean squared error (NRMSE) metric between the predicted system states and the ground truth. This metric quantifies the discrepancy in system states following the application of the predicted control commands across multiple time steps and is given as

$$\mathcal{N}_{i,K_p}^s = \frac{\frac{1}{K_p} \sum_{k=K_s+1}^{K_s+K_p} \sqrt{\|\tilde{\mathbf{x}}_{i,k} - \mathbf{x}_{i,k}\|_2^2}}{\|\max(\mathbf{x}) - \min(\mathbf{x})\|_2}, \quad (25)$$

where \mathcal{N}_{i,K_p}^s is the NRMSE of the device i at time k for K_p time steps.

To ascertain the efficiency of compressing input frame size $|\mathcal{I}_{i,k}|$ into encoded semantic representations $|\mathbf{z}_{i,k}|$ for conserving wireless communication resources, we quantify the compression ratio \mathcal{CR} between the original frame and its encoded counterpart as

$$\mathcal{CR} = 1 - \frac{d}{|\mathcal{I}|}, \quad (26)$$

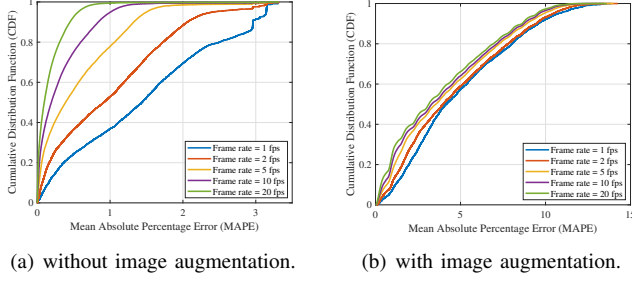


Fig. 5. Cumulative distribution function of the mean absolute percentage error between two consecutive frames with and without image augmentations.

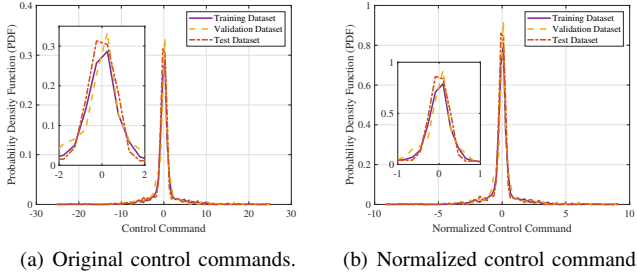


Fig. 6. Original and normalized control commands of the inverted cart-pole system for training, validation, and test datasets.

where $|\mathcal{I}|$ and d denote the cardinality of the frame and its corresponding semantic representations, respectively.

A. Performance Evaluation of Predictive Remote Control

We evaluate our approach on inverted cart-pole systems with uplink transmission from sensors to remote controllers. All results are averaged over 25 evaluation trajectories and repeated 5 times with different random seeds.

1) *TS-JEPA model Evaluation:* Fig.7 illustrates the first two components of the t-SNE analysis for the encoder and predictor within the trained TS-JEPA model. This visualization validates that the trained TS-JEPA model avoids converging to a naive solution, specifically one where distinct frames are mapped to a singular point or confined to a small region within the semantic space. As depicted in Fig.7, the t-SNE components exhibit a clear separation across a range from -100 to 100 , indicating that the trained model effectively captures the intrinsic structure of the depth frames and learns meaningful representations.

2) *Evaluating Encoding Capability of TS-JEPA Model:* Fig. 8 demonstrates a sequence of three frames, captured from time step 1 to 100 and at SNR values of 5 dB and 20 dB for both the expert and predictive models. While the frames from the proposed predictive model closely resemble the expert model across varying SNR values, the predictive model achieves the pendulum-up position more swiftly. However, this efficiency comes at the expense of increased control costs. This distinction is highlighted in Fig. 9, where the predicted control commands exhibit more variability than the target commands.

This result can be attributed to the ability of the proposed predictive remote control approach to extract semantic representations at the sensor end through the online encoder of

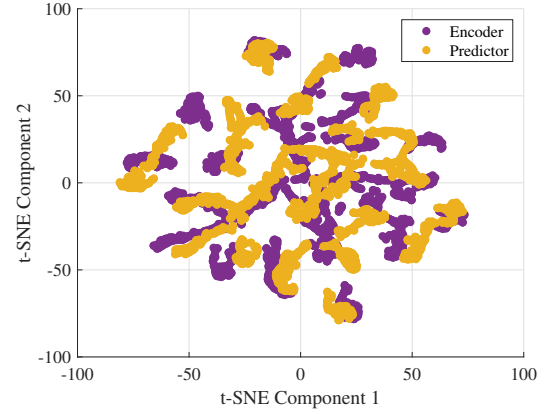


Fig. 7. t-SNE of the encoder and predictor of the TS-JEPA model.

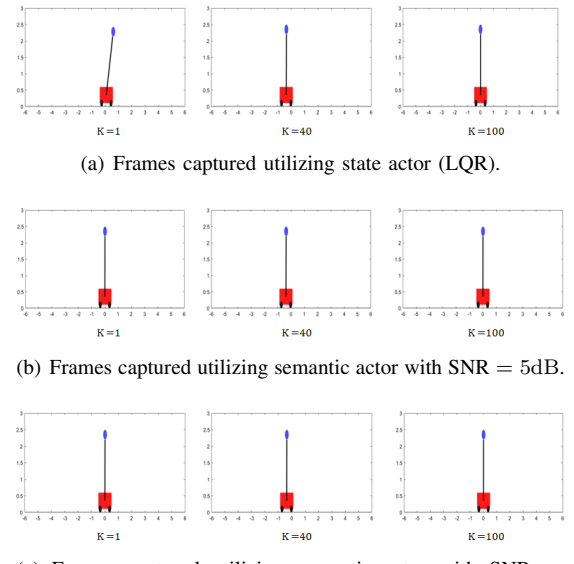


Fig. 8. Captured frames for the expert and predictive models at different SNR of 5 dB and 20 dB over a trajectory length of 100 time-steps.

the trained TS-JEPA model and transmit them wirelessly to the cloud server. Subsequently, the semantic actor at the cloud server predicts control commands based on these representations, which are then applied by the actuator. In cases of optimal control that balances between the control cost and state deviation cost, the actuator applies control commands optimized by the state actor utilizing LQR approach. It is clear in Fig. 9 that the predicted control commands by the proposed semantic actor in the first 10 time steps deviate from the optimal control commands calculated by the state actor at different SNR values. During training, varying SNRs of 5 dB and 20 dB influence the received training samples at the cloud server, with packet losses of approximately 1% and 30% at 20dB and 5dB, respectively. As the SNR decreases, the predicted control commands deviate from the optimal control command with a high std. Despite these challenges, the proposed predictive model demonstrates robustness across different SNR values.

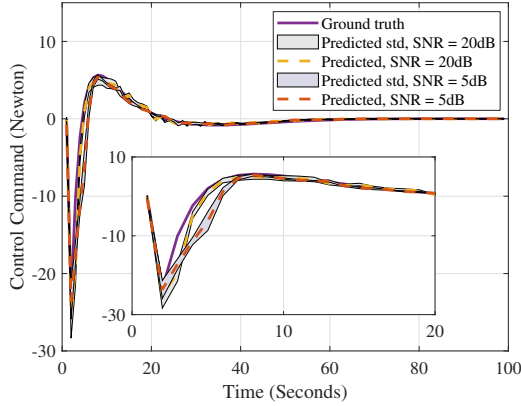
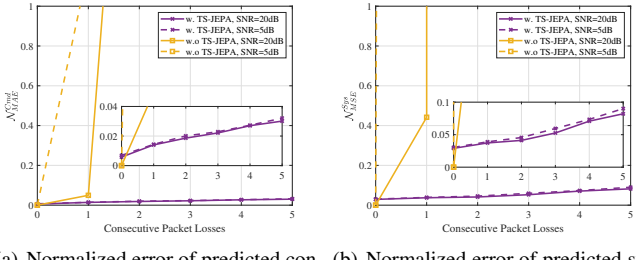


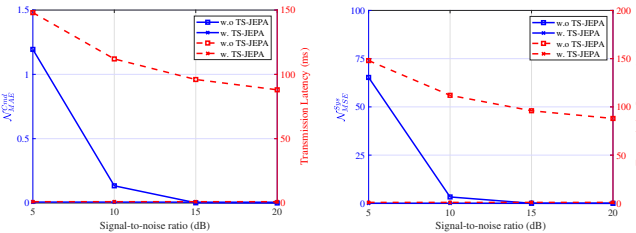
Fig. 9. Target and predicted control commands over time for the state and semantic actors, respectively at different SNR of 5 dB and 20 dB.



(a) Normalized error of predicted control commands. (b) Normalized error of predicted system states.

Fig. 10. Normalized error of predicted control commands (N_{MAE}^{Cmd}) and predicted system states (N_{MSE}^{Syst}) over consecutive packet losses for the proposed and baseline models at different SNR values of 5 dB and 20 dB.

3) *Evaluating Predicting Capability of TS-JEPA Model:* Fig. 10 illustrates the normalized errors between predicted and target control commands (Fig. 10(a)) and predicted system states and ground-truth (Fig. 10(b)) over consecutive packet losses and various SNR values for both the proposed predictive model with TS-JEPA and the baseline model without TS-JEPA. In Fig. 10(a), it is evident that the normalized control error of the proposed model with TS-JEPA remains consistent across different consecutive packet losses, contrasting with the baseline model without TS-JEPA, which exhibits an exponential growth in error after the first packet loss. This



(a) Normalized error of predicted control commands. (b) Normalized error of predicted system states.

Fig. 11. Transmission latency and normalized error of predicted control commands(N_{MAE}^{Cmd}) and predicted system states (N_{MSE}^{Syst}) over different SNR values for the proposed and baseline models.

behavior can be attributed to the TS-JEPA's ability to extract meaningful representations using the online encoder at the sensor side and transmit them to the cloud server, where the semantic actor predicts control commands from these received representations. In scenarios where devices are unscheduled or experience adverse channel conditions, the proposed model leverages the predictor of the TS-JEPA to predict the missing semantic representations at the cloud server, followed by control command calculation by the semantic actor.

The proposed predictive model employs an autoregressive approach, applying previously predicted representations and control commands to predict subsequent representations. The first five predicted representations in Fig. 10(a) yield control commands with a normalized error below 0.4% compared to the baseline model. Conversely, the baseline model struggles to compensate for missing frames in unscheduled or experiences adverse channel conditions, leading to inaccurate control predictions. Moreover, reducing SNR from 20 dB to 5 dB during testing exacerbates control prediction inaccuracies due to higher packet loss rates, which are approximately 1% and 30% at 20 dB and 5 dB SNR levels, respectively.

After achieving precise control command predictions with minimal error utilizing the TS-JEPA model and semantic actor, it is essential to verify whether these commands are adequate for maintaining the pendulum in the up position, as even slight variations in control can impact device stability. To assess this, Fig. 10(b) illustrates the normalized error between the predicted system states and ground truth, serving as a measure of control adequacy. The results depicted in Fig. 10(b) reveal that the proposed predictive model achieves a normalized error of 5% after three consecutive packet losses and 8.5% after five consecutive packet losses at SNR of 20 dB. This implies that, when aiming for 5% normalized error from the desired state, the proposed predictive model can compensate for up to three packet losses at SNR of 20 dB and up to two packet losses at SNR of 5 dB. Conversely, with the baseline model, if the normalized error between the predicted and target control commands exceeds 4% at the first packet loss, it leads to 40% normalized error between the predicted and ground-truth system states at SNR of 20 dB, significantly jeopardizing device stability during the trajectory. It is evident that even slight inaccuracies in predicted control commands significantly impact system accuracy.

4) *Evaluating Model Robustness:* Fig. 11 presents an analysis encompassing transmission latency alongside normalized errors between predicted and target control commands (Fig. 11(a)) and predicted system states and ground truth (Fig. 11(b)) across various SNR values. Notably, as the SNR value increases, both transmission latency and normalized errors decrease. This trend can be attributed to differences in frame resolution and transmission requirements between the baseline model without TS-JEPA and the proposed predictive model employing TS-JEPA. Specifically, the baseline model, featuring a frame resolution of $600 \times 1200 \times 3$ pixels with 32 bits per pixel, while the proposed model necessities transmission of a vector of length 256 elements and 32 bits per element. Given a total measurement bandwidth of 20 MHz with a guard band occupying 10% of the bandwidth, there are

100 available PRBs for transmission. The transmission latency is then determined based on the required resource blocks, each spanning 1 ms time interval, with the condition that the latency remains $10x$ faster than the control system's sampling rate to maintain device stability. At a SNR of 5 dB, the baseline model incurs a transmission latency of approximately 150 ms, resulting in delayed system updates and degraded control performance (Fig. 11). Conversely, increasing the SNR value to 15 dB reduces the latency below 100 ms, enhancing control performance. In contrast, the proposed predictive model, despite achieving a 99 compression ratio relative to the baseline, maintains robust control performance by extracting meaningful semantic representations with TS-JEPA at the cloud server, thus minimizing transmission latency without sacrificing task significance. This stands in stark contrast to conventional source coding methods, which often collapse data into representations lacking inherent meaning, thereby compromising task learning and performance.

VI. CONCLUSION

In this study, we have demonstrated the effectiveness of *Time-Series Joint Embedding Predictive Architecture* (TS-JEPA) in reducing traffic load while maintaining high performance in wireless control tasks under capacity-limited networks. By leveraging self-supervised learned representations, TS-JEPA extracts semantic representations of high-dimensional inputs at the sensor side and predicts missing representations at the controller side. This approach enables the remote prediction of the next representations, compensating for missing sensor inputs in capacity-limited uplink scenarios. The semantic actor then computes control commands based on these representations. Our simulation results show that TS-JEPA outperforms existing baselines in terms of effectiveness and scalability. However, future research directions include investigating the reliability of predicted representations in non-deterministic control problems and exploring the global network performance with advanced scheduling mechanisms.

REFERENCES

- [1] K. Lu, Q. Zhou, R. Li, Z. Zhao, X. Chen, J. Wu, and H. Zhang, "Rethinking modern communication from semantic coding to semantic communication," *IEEE Wireless Communications*, vol. 30, no. 1, pp. 158–164, 2023.
- [2] J. He, K. Yang, and H.-H. Chen, "6G cellular networks and connected autonomous vehicles," *IEEE network*, vol. 35, no. 4, pp. 255–261, 2020.
- [3] L. Ismail and R. Buyya, "Artificial intelligence applications and self-learning 6G networks for smart cities digital ecosystems: Taxonomy, challenges, and future directions," *Sensors*, vol. 22, no. 15, p. 5750, 2022.
- [4] R. T. Azuma, "A survey of augmented reality," *Presence: teleoperators & virtual environments*, vol. 6, no. 4, pp. 355–385, 1997.
- [5] P. Popovski, c. Stefanovic, J. J. Nielsen, E. de Carvalho, M. Angelichinoski, K. F. Trillingsgaard, and A.-S. Bana, "Wireless access in Ultra-Reliable Low-Latency Communication (URLLC)," *IEEE Transactions on Communications*, vol. 67, no. 8, pp. 5783–5801, 2019.
- [6] C. Bockelmann, N. Pratas, H. Nikopour, K. Au, T. Svensson, C. Stefanovic, P. Popovski, and A. Dekorsy, "Massive machine-type communications in 5G: Physical and MAC-layer solutions," *IEEE communications magazine*, vol. 54, no. 9, pp. 59–65, 2016.
- [7] G. Wang, C. Li, W. Wang, Y. Zhang, D. Shen, X. Zhang, R. Henao, and L. Carin, "Joint embedding of words and labels for text classification," *arXiv preprint arXiv:1805.04174*, 2018.
- [8] T. Chen, S. Kornblith, M. Norouzi, and G. Hinton, "A simple framework for contrastive learning of visual representations," in *International conference on machine learning*. PMLR, 2020, pp. 1597–1607.
- [9] Y. LeCun, "A path towards autonomous machine intelligence version 0.9. 2, 2022-06-27," *Open Review*, vol. 62, 2022.
- [10] M. Assran, Q. Duval, I. Misra, P. Bojanowski, P. Vincent, M. Rabbat, Y. LeCun, and N. Ballas, "Self-supervised learning from images with a joint-embedding predictive architecture," *arXiv preprint arXiv:2301.08243*, 2023.
- [11] J.-B. Grill, F. Strub, F. Altché, C. Tallec, P. Richemond, E. Buchatskaya, C. Doersch, B. Avila Pires, Z. Guo, M. Gheshlaghi Azar *et al.*, "Bootstrap your own latent a new approach to self-supervised learning," *Advances in neural information processing systems*, vol. 33, pp. 21271–21284, 2020.
- [12] P. Vepakomma, O. Gupta, T. Swedish, and R. Raskar, "Split learning for health: Distributed deep learning without sharing raw patient data," *arXiv preprint arXiv:1812.00564*, 2018.
- [13] A. Bardes, Q. Garrido, J. Ponce, X. Chen, M. Rabbat, Y. LeCun, M. Assran, and N. Ballas, "V-jepa: Latent video prediction for visual representation learning," 2023.
- [14] J. P. Hespanha, P. Naghshtabrizi, and Y. Xu, "A survey of recent results in networked control systems," *Proceedings of the IEEE*, vol. 95, no. 1, pp. 138–162, 2007.
- [15] D. Han, J. Wu, H. Zhang, and L. Shi, "Optimal sensor scheduling for multiple linear dynamical systems," *Automatica*, vol. 75, pp. 260–270, 2017.
- [16] M. Eisen, M. M. Rashid, D. Cavalcanti, and A. Ribeiro, "Control-aware scheduling for low latency wireless systems with deep learning," in *2020 IEEE International Conference on Communications Workshops (ICC Workshops)*. IEEE, 2020, pp. 1–7.
- [17] Y. Yu, X. Si, C. Hu, and J. Zhang, "A review of recurrent neural networks: LSTM cells and network architectures," *Neural computation*, vol. 31, no. 7, pp. 1235–1270, 2019.
- [18] J. Chung, C. Gulcehre, K. Cho, and Y. Bengio, "Empirical evaluation of gated recurrent neural networks on sequence modeling," *arXiv preprint arXiv:1412.3555*, 2014.
- [19] K. Ogata *et al.*, *Modern control engineering*. Prentice hall Upper Saddle River, NJ, 2010, vol. 5.
- [20] M. S. Fadali and A. Visioli, *Digital control engineering: analysis and design*. Academic Press, 2012.
- [21] A. Varghese and D. Tandur, "Wireless requirements and challenges in industry 4.0," in *2014 international conference on contemporary computing and informatics (IC3I)*. IEEE, 2014, pp. 634–638.
- [22] A. Goldsmith, *Wireless communications*. Cambridge university press, 2005.
- [23] T. ETSI, "138 901 v16. 1.0," *Study on channel model for frequencies from 0.5 to*, vol. 100, 2020.
- [24] T. Jiang, J. Zhang, P. Tang, L. Tian, Y. Zheng, J. Dou, H. Asplund, L. Raschkowski, R. D'Errico, and T. Jämsä, "3GPP standardized 5G channel model for IIoT scenarios: A survey," *IEEE Internet of Things Journal*, vol. 8, no. 11, pp. 8799–8815, 2021.
- [25] R. Szeliski, *Computer vision: algorithms and applications*. Springer Nature, 2022.
- [26] A. Bruhn, J. Weickert, and C. Schnörr, "Lucas/kanade meets horn/schunck: Combining local and global optic flow methods," *International journal of computer vision*, vol. 61, pp. 211–231, 2005.
- [27] A. Dosovitskiy, P. Fischer, E. Ilg, P. Hausser, C. Hazirbas, V. Golkov, P. Van Der Smagt, D. Cremers, and T. Brox, "Flownet: Learning optical flow with convolutional networks," in *Proceedings of the IEEE international conference on computer vision*, 2015, pp. 2758–2766.
- [28] E. Ilg, N. Mayer, T. Saikia, M. Keuper, A. Dosovitskiy, and T. Brox, "Flownet 2.0: Evolution of optical flow estimation with deep networks," in *Proceedings of the IEEE conference on computer vision and pattern recognition*, 2017, pp. 2462–2470.
- [29] T.-W. Hui, X. Tang, and C. C. Loy, "Liteflownet: A lightweight convolutional neural network for optical flow estimation," in *Proceedings of the IEEE conference on computer vision and pattern recognition*, 2018, pp. 8981–8989.
- [30] P. Morasso, T. Nomura, Y. Suzuki, and J. Zenzeri, "Stabilization of a cart inverted pendulum: improving the intermittent feedback strategy to match the limits of human performance," *Frontiers in computational neuroscience*, vol. 13, p. 16, 2019.